Refractive index measured by laser beam displacement at $\lambda = 1064\,\text{nm}$ for solvents and deuterated solvents

David P. Shelton

Department of Physics and Astronomy, University of Nevada, Las Vegas,
Nevada 89154-4002, USA (shelton@physics.unlv.edu)

The refractive index of a liquid is determined with 0.0003 accuracy from measurements of laser beam displacement by a liquid-filled standard 10 mm spectrophotometer cell. The apparatus and methods are described and the results of measurements at $\lambda = 1064\,\text{nm}$ and $T = 25.0\,°C$ for 30 solvents and deuterated solvents are presented. Several sources of potential systematic errors as large as 0.003 are identified, the most important being the curvature of the liquid cell windows. The measurements are analyzed accounting for the significant imperfections of the apparatus. © 2011 Optical Society of America
OCIS codes: 120.3930, 120.3940, 120.4530, 120.4570, 160.4760, 160.4890.

1. Introduction

The refractive index very often enters the analysis of optical experiments, and it was the need for refractive index values in the analysis of hyper-Rayleigh scattering measurements for liquid solvent samples that provided the motivation for the present work [1]. Accurate refractive indices n for liquid solvents measured at the 1064 nm Nd:YAG laser wavelength are usually unavailable from the literature, so a simple apparatus was constructed to measure n. Many techniques have been proposed and used to measure the refractive index [2–17]. The beam displacement method [2] appeared most suitable since it is especially simple and direct and the apparatus can be assembled from readily available standard components. However, the method as originally proposed [2] did not produce reliable results. The origin of the problem and the necessary refinement of the method to obtain reliable results are the subject of the present work.

The beam displacement method for measuring the refractive index of a liquid, as previously described, obtains the refractive index of a plane parallel slab from measurements of the transverse displacement of a beam obliquely incident on the slab [2]. The liquid sample is contained in a standard rectangular spectrophotometric cell with nominally plane parallel windows, and the transverse displacement of a laser beam in the horizontal plane of incidence is measured as the cell is rotated about the vertical axis through the center of the cell. The displacement versus rotation angle is measured first for the empty cell and then for the cell filled with the sample liquid. The refractive index of the liquid is determined from the difference Δ between filled and empty cell beam displacements. The refractive index and thickness of the windows does not appear in the expression for the displacement difference

$$\Delta = d_2 \sin\theta [1 - n_0 \cos\theta / (n_2^2 - n_0^2 \sin^2\theta)^{1/2}], \quad (1)$$

where θ is the angle of incidence on the first surface, n_2 and n_0 are the refractive indices for the liquid fill and the surrounding air, and d_2 is the interior length of the cell. Solving Eq. (1) for n_2 gives

$$n_2 = n_0 \sin\theta [1 + \cos^2\theta / (\sin\theta - \Delta/d_2)^2]^{1/2}. \quad (2)$$

The values of n_2 obtained using Eq. (2) at several angles θ were simply averaged in [2]. The method is simple and the absolute refractive index is determined directly from position and angle measurements. The use of standard commercially available

spectrophotometer cells is attractive since the cells are transparent over a wide wavelength range, they are compatible with most liquids, and only a small sample is needed. The aim of the present work is to improve the accuracy of the refractive index results while preserving the simplicity and general applicability of the method.

2. Experimental Apparatus

Figure 1 shows a schematic diagram of the present apparatus. The beam from a diode-pumped single-longitudinal-mode Nd:YAG laser ($\lambda = 1064\,\text{nm}$) is expanded and collimated by a telescope, and a narrow beam is formed using either iris 1 or iris 2 (placed 60 and 8 cm from the sample cell, respectively). The narrow collimated beam propagates through the sample cell mounted on a rotation stage and is incident on the four-quadrant silicon photodetector (4QD) mounted on a translation stage (5 cm behind the sample cell). Moving the 4QD to make the difference between the signals from the left and right halves of the 4QD go to zero centers it on the beam, and the displacement of the centered 4QD measures the displacement of the beam as the sample cell is rotated. The sample cell is maintained at $T = 25.0\,°\text{C}$ by contact with a temperature-regulated aluminum holder, and a cylindrical shroud with a narrow horizontal slit maintains an isothermal zone around the cell while allowing beam access to the cell over a $\pm 40°$ angular range. The cell is initially oriented normal to the incident laser beam ($\theta < 0.1°$) by opening iris 2 and closing iris 1 to narrow the beam and then retro-reflecting the beam from the cell back onto iris 1. The beam displacement measurements are made with iris 1 open and with iris 2 closed to produce a 0.7 mm diameter, 0.5 mW beam (placing iris 2 and the 4QD close to the cell minimizes the effect of laser beam pointing fluctuations and drift). The 4QD can be set to the middle of this beam with submicrometer position sensitivity, and a digital readout micrometer gives the translation stage position with 0.001 mm accuracy. The reproducibility of the rotation stage angular settings is 0.01°.

The sample cells are standard 10 mm path length absorption or fluorescence cells with nominally 1.25 mm thick windows of synthetic fused silica glass (Heraeus Spectrosil), from Hellma, Spectrocell, or Starna. Typical specifications are $10.00 \pm 0.01\,\text{mm}$ for the path length between the windows, and window parallelism and flatness better than 3 arc min and 4 Newton fringes [18]. The refractive index of the fused silica window material is very reproducible and well characterized (variation $<3 \times 10^{-5}$) [19]. Based on data from the manufacturer for Heraeus Spectrosil, at $\lambda = 1064\,\text{nm}$ and $T = 25\,°\text{C}$ the refractive index is $n = 1.44968$ and $dn/dT = 9.6 \times 10^{-6}\,\text{K}^{-1}$ [20]. The refractive index is 1.00025 for air [21]. Several simple measurements were made to further characterize four individual cells. The distance d between the outer window surfaces was measured with 0.001 mm accuracy using a micrometer caliper. The angles between each of the window surfaces of the cell were measured with 0.003° resolution by reflecting a narrow collimated visible laser beam from the cell tilted a few degrees from normal incidence and observing the reflected beam spots on a screen placed 4 m from the cell. The wedge angle between the surfaces of a window was as large as 0.2°, while the angle between the inside surfaces of the two windows of a cell was usually $<0.02°$. Some of the cells had windows with nearly parallel surfaces, and in this case the window wedge angle was measured using wedge interference fringes.

Deviation from flatness for the outer window surfaces was measured using interference fringes obtained by placing the cell against an optical flat. The curvature of the outer window surfaces varied from cell to cell, and the curvature could be nearly uniform or highly variable over the surface of a window. The deviation from flat across the 12 mm width of a window varied from 0.7 μm convex to 0.7 μm concave, sometimes all on the same window. The observation of straight wedge fringes from windows with curved outer surfaces indicates that the windows start with nearly flat surfaces and that the observed curvature results from bending of the thin windows during assembly of the cell. On this basis, it is assumed that both sides of a window have the same curvature. Table 1 shows dimensions, as defined in Fig. 1, measured for two of the cells that were used in this work. The curvature of the front or back window (c_F or c_B)
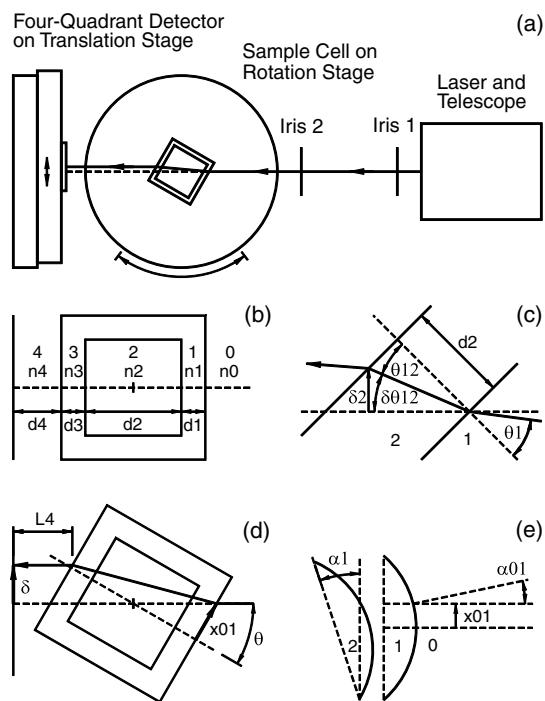

Fig. 1. Schematic diagrams showing (a) the overall configuration of the apparatus viewed from above and (b)–(e) more detailed diagrams defining the parameters and variables in Table 1 and Eqs. (8)–(11). The beam propagates right to left and the sign conventions are such that the angles θ, θ_1, θ_{12}, $\delta\theta_{12}$, α_1, and α_{01}, and displacements δ, δ_2, and x_{01} are all positive as drawn.

Table 1. Parameters Measured for Two Sample Cells

cell	1	2
source	Starna	Hellma
d (mm)	12.278	12.254
α_1 (°)	0.00	0.00
α_2 (°)	−0.01	0.06
α_3 (°)	0.00	−0.13
c_F (°/mm)	0.0022	−0.0025
c_B (°/mm)	0.0016	−0.0013

given in Table 1 is the average spatial derivative of the surface slope (degrees per millimeter) measured along the horizontal path sampled by the laser beam during the beam displacement measurements, and is taken as positive for a surface that is convex outward. The curvature uncertainty due to the measurement uncertainty of 0.25 fringe at $\lambda = 546$ nm is ±0.0002 °/mm. Cell 1 has convex cylindrical surfaces with nearly constant curvature, whereas each surface of cell 2 is first concave, then convex, then concave again, going from bottom to top of the cell (35 mm). The curvature uncertainty is larger for cell 2 due to the rapid variation of curvature with height.

3. Analysis

The sample cell has overall thickness $d = d_1 + d_2 + d_3$ with windows of thickness $d_1 = d_3$ separated by a distance d_2, and the cell is placed a distance d_4 from the detector plane, as shown in Fig. 1(b). The refractive indices of the surrounding air, the cell windows, and the cell interior are $n_0 = n_4$, $n_1 = n_3$ and n_2, respectively. In the case that all cell surfaces are plane parallel, a beam incident at angle θ on the first surface of the cell emerges from the cell parallel to the incident beam, but displaced. The beam displacement by layer 2 is illustrated in Fig. 1(c). The beam is incident at angle θ_1 with respect to the 1–2 surface normal and exits at angle θ_{12}. The beam in medium 2 propagates at angle $\delta\theta_{12} = \theta - \theta_{12}$ with respect to the direction of the beam incident on the cell, and the displacement by layer 2 is

$$\delta_2 = d_2 \sin(\delta\theta_{12})/\cos(\theta_{12}). \quad (3)$$

The total displacement at the detector plane is $\delta = \delta_1 + \delta_2 + \delta_3 + \delta_4$, where the expressions for the displacements δ_1 and δ_3 in the windows have the same form as Eq. (3) and the displacement as the beam propagates from the cell to the detector $\delta_4 = 0$. The expression previously derived for the beam displacement by a plane parallel cell is [2]

$$\delta = (d_1 + d_3) \sin\theta[1 - n_0 \cos\theta/(n_1^2 - n_0^2 \sin^2\theta)^{1/2}]$$
$$+ d_2 \sin\theta[1 - n_0 \cos\theta/(n_2^2 - n_0^2 \sin^2\theta)^{1/2}]. \quad (4)$$

The predicted displacement is $\delta = 2.2$ mm at $\theta = 30°$ for a 10 mm cell filled with liquid CCl_4 (which nearly matches the refractive index of the windows). The displacement change is $\Delta\delta = 0.001$ mm for a change $\Delta n = 0.0003$ in the refractive index, so, conversely, to determine the refractive index with 0.0003 accuracy, the displacement must be determined with 0.001 mm accuracy.

Interference between the beams reflected from the surfaces of the cell can cause significant errors in the beam position and displacement measurements. Interference between the reflections from a pair of plane parallel surfaces causes the intensity of the transmitted beam to change by a factor $(1 - A\cos\phi)$, where A is the amplitude of the intensity modulation and ϕ is the phase difference between the reflected beams. For two interfaces with reflection coefficients R_1 and R_2, the amplitude $A = 2(R_1 R_2)^{1/2}$, so $A = 0.07$ for a pair of air-fused silica interfaces. Interference only occurs where the reflected beams overlap, and the overlap between the narrow reflected beams decreases as the cell is rotated away from normal incidence. The partial overlap of the reflected beams results in a step in the intensity profile of the transmitted beam. The 4QD is set to the position where the integrated intensities of the beam on the left and right halves of the detector are equal (the null position or "middle"), so the intensity step due to the interference of the overlapping reflected beams causes a shift x_m in the position determined by the 4QD. For a square beam spot with width D and reflections with fractional overlap F, the shift x_m is $x_m = -A\cos\phi FD/2$ for $F \leq 1/2$, and $x_m = -A\cos\phi(1 - F)D/2$ for $F \geq 1/2$, where positive x_m is a shift toward the reflected beams. The maximum shift is $x_m = AD/4$, which for $A = 0.07$ and $D = 0.7$ mm gives a position error $x_m = 0.012$ mm.

In the case that there is a small wedge angle α between the surfaces, the intensity of the transmitted beam centered at $x = 0$ will be modulated by a spatially varying factor

$$I(x) = 1 + A\sin K(x - x_0), \quad (5)$$

where $K = 2\pi/\Lambda$ and $\Lambda = \lambda/(2n\alpha)$ is the period of the interference fringes. For a square beam spot of width D, the position determined by the 4QD will be shifted from the beam center by distance x_m, given by

$$x_m = (A/K)[\cos(Kx_m - Kx_0) - \cos(KD/2)\cos(Kx_0)]. \quad (6)$$

The worst case position shift is $x_m = AD/\pi$ for $x_0 = 0$ and $\Lambda = D$, which for $A = 0.07$ and $D = 0.7$ mm is $x_m = 0.016$ mm. For $n = 1.45$ and $\lambda = 1064$ nm, the worst case fringe period $\Lambda = D = 0.7$ mm is obtained for $\alpha = 0.5$ mrad $= 0.03°$, close to the 0.01° and 0.07° wedge angles measured between the outside faces for cells 1 and 2, respectively. Near normal incidence, the reflections from the outside faces of a liquid-filled cell will overlap and interfere, and one should expect beam position measurement errors of the order of $x_m = \pm0.016$ mm, resulting in errors of the order of ±0.005 for the refractive index. The overlap and interference between these reflected beams will disappear when the cell is rotated 5°, but the reflections

from the two surfaces of each window will overlap and interfere for $\theta \leq 25°$. However, the reduced reflection from the liquid–glass interface of a filled cell reduces A by a factor of 3–300, depending on the refractive index of the liquid, and this reduces the position error resulting from the interfering window reflections. Therefore, the least reliable beam position measurement is obtained at normal incidence and the refractive index determination will be inaccurate if it depends on the measured beam position at normal incidence.

The information needed to determine the refractive index is contained in the slope of the function $\delta(\theta)$ so the problem of the uncertain beam position near normal incidence is avoided by using a least squares fit to the measured δ_m versus θ_m data, not including the $\theta_m = 0$ point. The fit function f is constructed using Eq. (4) for $\delta(\theta)$:

$$f = \delta(\theta; n_2, \theta_0) + C. \tag{7}$$

The adjustable parameters for the fit are n_2, θ_0, and C, where $\theta = \theta_m + \theta_0$ relates the actual angle of incidence θ to the measured angle θ_m and C is the beam position at $\theta_m = 0$. This fit gives the correct weight to the beam displacement measurements made at different angles and the best fit value for n_2 is insensitive to the uncertainty of the angle of incidence and beam position at $\theta_m = 0$.

However, the surfaces of the actual cells are not parallel and flat, as was assumed in the derivation of Eq. (4), and as a result the beam is deviated and the displacement of the beam at the detector is changed. The beam displacement has been calculated by tracing the beam through the cell, accounting for the small changes in slope for the window surfaces but ignoring the changes in thickness. The wedge angles between successive surfaces (but not the surface curvatures) produce a cumulative change on the surface slope. The slope correction due to a wedge angle is constant across a window surface, but the slope correction due to curvature varies with transverse position on the window, as shown in Figs. 1(d) and 1(e). Thus, $\alpha_{01} = c_F x_{01}$ for the first window surface, where x_{01} is the beam position with respect to the center of the window and c_F is the curvature of the front window. For measurements over a $\pm 35°$ angular range, the length of the beam track across the front window of the cell will be 9 mm, nearly reaching the corners of the cell. The length of the beam track on the back window is shorter due to the beam displacement, which will reduce the effect of the curvature of the back window. The explicit expressions for calculating the beam displacement by the front window are as follows:

$$x_{01} = (d_1 + d_2/2)\tan\theta, \tag{8a}$$

$$\alpha_{01} = c_F x_{01}, \tag{8b}$$

$$\theta_{01} = \arcsin[(n_0/n_1)\sin(\theta - \alpha_{01})], \tag{8c}$$

$$\delta\theta_{01} = \theta - \theta_{01} - \alpha_{01}, \tag{8d}$$

$$\delta_1 = d_1 \sin(\delta\theta_{01})/\cos(\theta_{01}). \tag{8e}$$

The expressions for the beam displacement in the interior space between the windows are

$$x_{12} = (d_2/2)\tan\theta + \delta_1/\cos\theta, \tag{9a}$$

$$\alpha_{12} = c_F x_{12}, \tag{9b}$$

$$\theta_{12} = \arcsin[(n_1/n_2)\sin(\theta_{01} + \alpha_{01} - \alpha_{12} - \alpha_1)], \tag{9c}$$

$$\delta\theta_{12} = \theta - \theta_{12} - \alpha_{12} - \alpha_1, \tag{9d}$$

$$\delta_2 = d_2 \sin(\delta\theta_{12})/\cos(\theta_{12}). \tag{9e}$$

The expressions for the beam displacement by the back window are

$$x_{23} = -(d_2/2)\tan\theta + (\delta_1 + \delta_2)/\cos\theta, \tag{10a}$$

$$\alpha_{23} = -c_B x_{23}, \tag{10b}$$

$$\theta_{23} = \arcsin[(n_2/n_3)\sin(\theta_{12} + \alpha_{12} - \alpha_{23} - \alpha_2)], \tag{10c}$$

$$\delta\theta_{23} = \theta - \theta_{23} - \alpha_{23} - \alpha_1 - \alpha_2, \tag{10d}$$

$$\delta_3 = d_3 \sin(\delta\theta_{23})/\cos(\theta_{23}). \tag{10e}$$

The expressions for the beam displacement in the space between the cell and the detector are

$$x_{34} = -(d_3 + d_2/2)\tan\theta + (\delta_1 + \delta_2 + \delta_3)/\cos\theta, \tag{11a}$$

$$\alpha_{34} = -c_B x_{34}, \tag{11b}$$

$$\theta_{34} = \arcsin[(n_3/n_4)\sin(\theta_{23} + \alpha_{23} - \alpha_{34} - \alpha_3)], \tag{11c}$$

$$\delta\theta_{34} = \theta - \theta_{34} - \alpha_{34} - \alpha_1 - \alpha_2 - \alpha_3, \tag{11d}$$

$$L_4 = d_4 + (d_3 + d_2/2)(1 - 1/\cos\theta) + (\delta_1 + \delta_2 + \delta_3)\tan\theta, \tag{11e}$$

$$\delta_4 = L_4 \tan(\delta\theta_{34}). \tag{11f}$$

Total displacement at the detector plane is

$$\delta(\theta) = \delta_1 + \delta_2 + \delta_3 + \delta_4. \tag{12}$$

It is straightforward to perform the least squares fit to the measured beam displacements using the fit function f obtained by substituting the function $\delta(\theta)$ defined by Eqs. (8)–(12) into Eq. (7). The refractive index n_2, obtained from such a fit, for data covering an angular range symmetric about $\theta = 0$ is sensitive to the curvature of the window surfaces but insensitive to the wedge angles. The effect of a small wedge angle between surfaces is to produce a deviation of the exit beam, where minimum deviation occurs near

normal incidence. There is little effect on n_2 since the deviation is an even function of θ that shifts the $\delta(\theta)$ curve without changing the average slope. In contrast, the beam deflection due to window curvature has a large effect on n_2 since the deviation is an odd function of θ. For a 10 mm cell filled with liquid CCl_4, the error in n_2 due to 0.0025°/mm curvature error in the fit function is $\Delta n_2 = 0.002$ as compared to $\Delta n_2 = 0.0002$ due to 0.2° wedge angle error.

Another source of systematic error in n_2 is the uncertainty of the cell length. The 0.001 mm uncertainty for the overall cell length d results in 0.0001 uncertainty for n_2. The error due to 0.01 mm uncertainty for the interior path length d_2 is proportional to the difference between the liquid and window refractive indices and has a maximum value of 0.00015 for liquids with n_2 in the range 1.3–1.6. The window thickness can be determined by fitting Eqs. (7)–(12) to displacement measurements for the empty cell, and this result can be combined with the overall length measurement to determine the interior path length of the cell. The result so obtained is consistent with the manufacturer specifications for the cell and has about same the uncertainty.

A final source of systematic error in n_2 is the eccentricity of the angle scale on the rotation stage. In the present apparatus, the rotation angle is read on one side of the rotation scale using a CCD camera, and for such single-side readings the dominant error is often due to the eccentricity of the scale with respect to the rotation axis (averaging diametrically opposite readings eliminates this error). Corrected single-side angle readings are given by the expression

$$\theta_m = \theta'_m + E[\sin(\theta'_m + \phi_E) - \sin(\phi_E)], \qquad (13)$$

where θ'_m and θ_m are the angle readings before and after correction for the eccentricity error, E is the maximum angle error due to the eccentricity of the angular scale with respect to the rotation axis, and ϕ_E is the angle of the line from the center of the scale to the rotation axis [22]. The parameters E and ϕ_E may be determined from measurements using a plane parallel block on the rotation stage and an autocollimator, or without additional instruments from four sets of beam displacement measurements on the same sample with the scale origin advanced by 90° for each successive set. The requirement that the four sets return the same best fit value for n_2 is used to determine the parameters E and ϕ_E. The maximum eccentricity correction for the rotation stage used in this work is 10× larger than the setting precision for the rotation stage.

4. Results and Discussion

Figure 2 shows typical measurements of beam displacement versus cell rotation angle made with this apparatus. The reproducibility of the measurements is at the limit set by the 1 μm reading resolution of the digital micrometer on the 4QD translation stage and the statistical uncertainty is ± 0.0001 for n_2 ob-

tained from the least squares fit to the data shown in Fig. 2. However, there appears to be a significant systematic variation of the residual differences between the data and the fit, which could indicate a significant systematic error for n_2. This is considered below.

A possible source for the trend in the residuals seen in Fig. 2 is deviation from constant curvature across the width of the window. The effect of window curvature variation has been investigated by fitting the data with an augmented model for the cell. Variation in window curvature is modeled by adding terms quadratic and cubic in the beam position to Eqs. (8b), (9b), (10b), and (11b), and decentering of the cell with respect to the rotation axis is modeled by adding the term $\delta_0/\cos\theta$ to Eqs. (8a), (9a), (10a), and (11a). The systematic variation of the residuals can be reduced to zero for the fit to the measurements in Fig. 2 by introducing a linear variation of the curvature across the front window of the cell into the fit function. While there is no significant change in the best fit n_2 value for the centered cell, the fitted value for θ_0 is much too large and the value of n_2 becomes sensitive to decentering of the cell since this now changes the average curvature. The curvature variation needed to force a fit to the data gives an asymmetry in the surface slope that is 10× too large to be consistent with the surface profile determined from the observed fringe patterns. Curvature variations that are consistent with the directly measured profile are too small to account for the systematic
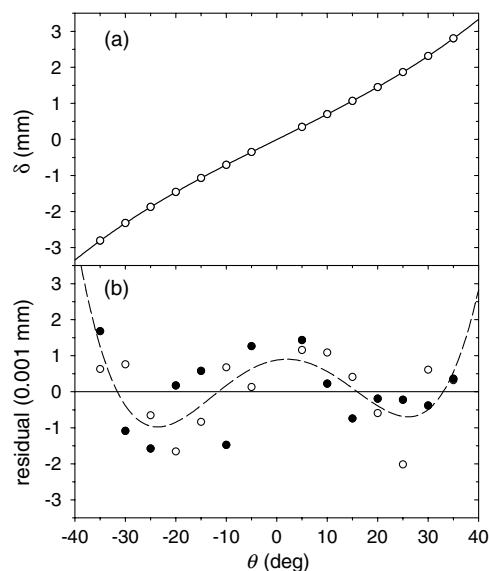

Fig. 2. (a) Beam displacement δ versus rotation angle θ for cell 1 filled with C_2Cl_4 measured at $\lambda = 1064$ nm and $T = 25.0$ °C. The open circles are the data and the solid curve is the fit to the data using the function defined by Eqs. (7)–(13). The value $n_2 = 1.4893 \pm 0.0001$ is obtained from the fit. (b) The residual differences between the data and the fit for two successive sets of measurements are shown by the open and filled circles. The standard deviation for the residuals is 1.0 μm. Systematic variation of the residuals is indicated by the polynomial fit to the residuals (dashed curve).

Table 2. Refractive Index n and Refractive Index Difference $n_H - n_D$ Between Corresponding Normal and Deuterated Liquids at $\lambda = 1064\,nm$ and $T = 25\,°C$, with the Uncertainty for the Last Digit Given in Parentheses

name	formula	n cell 1 [a]	n cell 2 [b]	n literature	$n_H - n_D$
water	H_2O	1.3238(1)	1.3244(6)	1.3240(1)	
deuterated water	D_2O	1.3211(1)	1.3211(2)		0.0028(2)
methanol	CH_3OH		1.3198(3)		
methanol-d	CH_3OD		1.3190(2)		0.0008(4)
methanol-d4	CD_3OD		1.3173(3)		0.0025(4)
acetonitrile	CH_3CN		1.3354(3)		
acetonitrile-d3	CD_3CN		1.3329(5)		0.0025(6)
nitromethane	CH_3NO_2		1.3704(4)		
nitromethane-d3	CD_3NO_2		1.3697(3)		0.0007(5)
acetone	$(CH_3)_2CO$		1.3487(4)		
acetone-d6	$(CD_3)_2CO$		1.3462(4)		0.0025(6)
dimethyl sulfoxide	$(CH_3)_2SO$		1.4657(6)		
dimethyl sulfoxide-d6	$(CD_3)_2SO$		1.4638(9)		0.0019(11)
carbon disulfide	CS_2	1.5910(3)		1.5906(4)	
tetrachloroethylene	C_2Cl_4	1.4893(1)			
carbon tetrachloride	CCl_4	1.4477(2)			
chloroform	$CHCl_3$		1.4331(4) [c]	1.4331(4)	
chloroform-d	$CDCl_3$		1.4326(2)		0.0005(5)
dichloromethane	CH_2Cl_2		1.4120(5)		
benzene	C_6H_6	1.4814(1)	1.4808(5)	1.4811(4)	
benzene-d6	C_6D_6	1.4796(2)			0.0018(2)
toluene	$C_6H_5CH_3$	1.4784(1)	1.4777(3)	1.4783(4)	
toluene-d8	$C_6D_5CD_3$	1.4760(2)			0.0024(2)
nitrobenzene	$C_6H_5NO_2$	1.5262(2)			
nitrobenzene-d5	$C_6D_5NO_2$	1.5262(3)			0.0000(4)
perfluorobenzonitrile	C_6F_5CN	1.4254(4)			
cyclohexane	C_6H_{12}		1.4158(4)		
propylene carbonate	$CH_3C_2H_3CO_3$		1.4122(3)		
1,4-dioxane	$(CH_2)_4O_2$		1.4119(2)		
tetrahydrofuran	$(CH_2)_4O$	1.3974(1)			

[a] not including ± 0.0003 systematic uncertainty
[b] not including ± 0.0005 systematic uncertainty
[c] $n = 1.4325(3)$ before correction for 0.75% ethanol

variation of the residuals seen in Fig. 2 and do not introduce a significant systematic error for n_2.

Another possible source for the trend in the residuals is the beam position error due to interference fringes. At normal incidence, the effect of interference fringes is evident from the $20\,\mu m$ fluctuations in measured beam position observed as the liquid in the cell relaxes to the temperature set point, and then the smaller wander of the measured position that can be attributed to optical path length changes for the liquid between the windows due to temperature drifts of the order of $0.01\,°C$. The measurements made with $\theta \geq 5°$ are much more stable since the strong reflections from the outside faces of the cell no longer overlap and interfere. The modulation amplitude due to interference between the beams reflected at the nearly parallel air–silica and liquid–silica interfaces for each window of cell 1 filled with C_2Cl_4 is $A = 0.005$, resulting in beam position error contributions as large as $1\,\mu m$ from each window. The beam position error is predicted to oscillate rapidly with angle, but an apparently slow, smooth oscillation of the residuals results when the measurements are made at precise uniform angular intervals of $5°$. Thus, the predicted position error due to interference

fringes is of the correct size and can be made to vary with the same trend as the residuals seen in Fig. 2. The observed trend is due to coarse sampling of rapidly oscillating interference fringes. Therefore, the variation of the residuals is treated as random and the effect of the interference fringes is included in the statistical error estimates for the fit parameters.

The uncertainty for n_2 obtained from beam displacement measurements has a statistical contribution due to the measurement errors for the particular sample, which include reading errors for position and angle, and position errors due to interference fringes, and a systematic contribution due to errors in the cell model represented by the fit function, which includes errors in the measured window curvatures, wedge angles, and path lengths for the cell. The systematic error estimate for n_2 is ± 0.0003 for cell 1 and ± 0.0005 for cell 2, mainly due to the uncertainty of the window curvature. The uncertainty is larger for cell 2 because of the height dependence of the window curvature for this cell, and the angular range for measurements is also restricted to $\pm 30°$ to avoid the corners of this cell where the curvature changes abruptly.

Table 2 shows the results of refractive index measurements made for 30 liquids (11 deuterated and 19 ordinary solvents) using these two cells. The purity was >99.9% for all the liquids except CH_3NO_2 (99.7%), C_6F_5CN (99.4%), and $CHCl_3$ (which contains 0.75% ethanol as stabilizer), and the isotopic purity of the deuterated solvents was >99.5 at. %D except for CD_3NO_2 (99 at. %D). The refractive index uncertainty for each liquid is the sum of the statistical and systematic errors, but the systematic error contributions cancel out for the refractive index difference between the normal liquid and corresponding deuterated liquid ($n_H - n_D$) measured in the same cell under the same conditions. The effect of deuteration varies with the molecule, decreasing the refractive index by 0.0000–0.0028, and the differences $n_H - n_D$ measured at 1064 nm are about 0.001 smaller than the differences at $\lambda = 589.3$ nm and $T = 20\,°C$ found in the literature. The measured value in Table 2 for pure chloroform is obtained by estimating the effect of the 0.75% ethanol stabilizer in the $CHCl_3$ sample, using the refractive index difference 0.085 between chloroform and ethanol measured at $\lambda = 589.3$ nm and $T = 25\,°C$ [21]. The refractive indices of water, benzene, and toluene were measured using both cells. The n_2 results for the two cells differ by 0.0005 ± 0.0003, consistent with the 0.0006 combined systematic uncertainties and much smaller than the 0.004 difference in the effect of the opposite window curvatures for the two cells.

The refractive indices were also tested by comparison with values obtained from the literature for several of the liquids. A broad range of refractive index data for chloroform, toluene, benzene, and carbon disulfide has recently been collected and critically examined [23]. The refractive index at $\lambda = 1064$ nm is obtained from the dispersion curve fit to the ultraviolet, visible, and infrared data at $T = 20\,°C$ for each of these liquids (no measurements at $\lambda = 1064$ nm, standard deviation in the range 0.0003–0.0008) [23], and the refractive index at $25\,°C$ is obtained using literature values for dn/dT measured in the visible [3,6,9,23–26]. The refractive index is reduced ≈ 0.003 due to $dn/dT \approx -6 \times 10^{-4}\,K^{-1}$ for these liquids, and since there are discrepancies as large as 20% in the reported values for dn/dT, the temperature adjustment uncertainty can be the largest contribution to the 0.0004 uncertainty estimated for the literature n values given in Table 2 for these liquids. The literature value for the refractive index of water at $\lambda = 1064$ nm and $T = 25\,°C$ in Table 2 is based on the result $n = 1.3238 \pm 0.0002$ obtained from recent measurements at 1064 nm for a temperature range including $25\,°C$ [4] and the result $n = 1.3241 \pm 0.0001$ from more recent measurements at wavelengths around 1064 nm and a range of temperatures near $25\,°C$ [5]. The refractive indices from the literature and from the present measurements agree to within the combined uncertainties for all five liquids. This is further evidence for the adequacy of the systematic error analysis.

In summary, refractive index measurements with ± 0.0003 accuracy and ± 0.0001 precision can be achieved using imperfect standard spectrophotometer cells in a compact apparatus constructed from off-the-shelf components, provided a few simple supplementary measurements are made to characterize the apparatus. The measurements used to determine the refractive index are simpler than in the previous work [2] since the beam position is determined as the null position for the four-quadrant detector signal and since empty-cell beam displacement measurements are not needed. The beam displacement by the liquid-filled cell is measured for several cell rotation angles and the refractive index is obtained from a least squares fit to the data using the beam displacement function for the cell. Cells with accurately flat windows would eliminate the leading systematic uncertainty due to window curvature, and the attainable accuracy would then be limited by cell dimension uncertainties and the beam displacement uncertainty due to interference fringes.

References

1. D. P. Shelton, "Nonlocal hyper-Rayleigh scattering from liquid nitrobenzene," J. Chem. Phys. **132**, 154506 (2010).
2. S. Nemoto, "Measurement of the refractive index of liquid using laser beam displacement," Appl. Opt. **31**, 6690–6694 (1992).
3. E. Moreels, C. de Greef, and R. Finsy, "Laser light refractometer," Appl. Opt. **23**, 3010–3013 (1984).
4. B. Richerzhagen, "Interferometer for measuring the absolute refractive index of liquid water as a function of temperature at $1.064\,\mu m$," Appl. Opt. **35**, 1650–1653 (1996).
5. M. Daimon and A. Masumura, "Measurement of the refractive index of distilled water from the near-infrared region to the ultraviolet region," Appl. Opt. **46**, 3811–3820 (2007).
6. J. Rheims, J. Koser, and T. Wriedt, "Refractive-index measurements in the near-IR using an Abbe refractometer," Meas. Sci. Technol. **8**, 601–605 (1997).
7. G. H. Meeten, "Refractive index errors in the critical-angle and Brewster-angle mehods applied to absorbing and heterogeneous materials," Meas. Sci. Technol. **8**, 728–733 (1997).
8. C.-B. Kim and C. Su, "Measurement of the refractive index of liquids at 1.3 and 1.5 micron using a fibre optic Fresnel ratio meter," Meas. Sci. Technol. **15**, 1683–1686 (2004).
9. A. Suhadolnik, "An optical fibre interferometric refractometer," Meas. Sci. Technol. **18**, 1205–1208 (2007).
10. B. Santic, D. Gracin, and K. Juraic, "Measurement method for the refractive index of thick solid and liquid layers," Appl. Opt. **48**, 4430–4436 (2009).
11. V. Greco, L. Hoffer, and G. Molesini, "Measuring the refractive index of thin liquid films with a spectrometer," Appl. Opt. **40**, 5111–5113 (2001).
12. R. Ramponi, R. Osellame, M. Marangoni, and V. Russo, "Near-infrared refractometery of liquids by means of waveguide Cerenkov second-harmonic generation," Appl. Opt. **37**, 7737–7742 (1998).
13. K. G. Muller, S. Sainov, S. Mittler-Neher, and W. Knoll, "Design and test of a simple high-temperature laser microrefractometer," Appl. Opt. **35**, 708–710 (1996).
14. C. Bahrim and W.-T. Hsu, "Precise measurements of the refractive indices for dielectrics using an improved Brewster angle method," Am. J. Phys. **77**, 337–343 (2009).

15. F. El-Ghussein, J. M. Wrobel, and M. B. Kruger, "Dispersion measurements with minimum and maximum deviated beams," Am. J. Phys. **74**, 888–891 (2006).

16. G. E. Hassan, H. El-Kashef, B. Y. El-Baradie, and M. El-Labban, "Interferometric measurement of the physical constants of laser dye solvents," Rev. Sci. Instrum. **66**, 38–42 (1995).

17. S. Singh, "Refractive index measurement and its applications," Phys. Scr. **65**, 167–180 (2002).

18. Starna Cells catalog for typical cell specifications, at www .starnacells.com.

19. I. H. Malitson, "Interspecimen comparison of the refractive index of fused silica," J. Opt. Soc. Am. **55**, 1205–1209 (1965).

20. Downloads for Spectrosil and Quartz Glass for Optics: Data and Properties, at http://heraeus-quarzglas.com.

21. *CRC Handbook of Chemistry and Physics*, 68th ed., R. C. Weast, ed. (CRC, 1987).

22. S. Qin, A. Huang, and X. Wang, "Optical angular encoder installation error measurement and calibration by ring laser gyroscope," IEEE Trans. Instrum. Meas. **59**, 506–511 (2010).

23. A. Samoc, "Dispersion of refractive properties of solvents: chloroform, toluene, benzene, and carbon disulfide in ultraviolet, visible, and near-infrared," J. Appl. Phys. **94**, 6167–6174 (2003).

24. D. Beysens and P. Calmettes, "Temperature dependence of the refractive indices of liquids: deviation from the Lorentz–Lorenz formula," J. Chem. Phys. **66**, 766–771 (1977).

25. M. Debenham and G. D. Dew, "The refractive index of toluene in the visible spectral region," J. Phys. E **14**, 544–545 (1981).

26. S. Valkai, J. Liszi, and I. Szalai, "Temperature dependence of the refractive index for three chloromethane liquids at 514.5 nm and 632.8 nm wavelengths," J. Chem. Thermodyn. **30**, 825–832 (1998).